Original Article
m6A methyltransferase METTL3 promotes oral squamous cell carcinoma progression through enhancement of IGF2BP2-mediated SLC7A11 mRNA stability

Le Xu[1], Qingxiang Li[1], Yifei Wang[1], Lin Wang[1], Yuxing Guo[1], Rong Yang[1], Na Zhao[2,3], Na Ge[1], Yixiang Wang[4], Chuanbin Guo[1]

[1]Department of Oral and Maxillofacial Surgery, Peking University School and Hospital of Stomatology & National Center of Stomatology & National Clinical Research Center for Oral Diseases & National Engineering Laboratory for Digital and Material Technology of Stomatology & Beijing Key Laboratory of Digital Stomatology & Research Center of Engineering and Technology for Computerized Dentistry Ministry of Health & NMPA Key Laboratory for Dental Materials, No. 22, Zhongguancun South Avenue, Haidian District, Beijing 100081, PR China; [2]Shanghai Stomatological Hospital, Fudan University, No. 356, Beijing Road East, Shanghai, PR China; [3]Dentistry and Biomaterials Sciences, Harvard School of Dental Medicine, Boston, Massachusetts, USA; [4]Central Laboratory, Peking University School and Hospital of Stomatology, No. 22, Zhongguancun South Avenue, Haidian District, Beijing 100081, PR China

Abstract: As the key enzyme of the N6-methyladenosine (m6A) in eukaryotic messenger RNA, METTL3 plays an important role in tumor progression, but the exact mechanism by which METTL3 controls oral squamous cell carcinoma (OSCC) progression remains unclear. In this study, METTL3 expression in OSCC samples was analyzed by qPCR and immunohistochemistry. The effects of METTL3 suppression on OSCC cell lines were measured by CCK-8, Ki67 flow cytometry analysis, invasion transwell and wound healing assays. MeRIP-seq and RNA-seq analyses were performed to explore target gene of METTL3. RIP-qPCR and RNA stability assays were performed to explore the mechanism by which METTL3 regulated the target genes. Triptolide was used to evaluate its specific treatment effects on METTL3 in OSCC cells. BALB/c nude mice were used to establish orthotopic and subcutaneous xenograft models to verify the in vitro results. The results showed that METTL3 was upregulated in OSCC tissues compared with OSCC adjacent normal tissues, and its expression was associated with T stage, lymphatic metastasis and prognosis. METTL3 suppression impaired OSCC cells proliferation, invasion, and migration. MeRIP-seq and RNA-seq analysis identified that SLC7A11 mRNA was the m6A target of METTL3, which was verified by meRIP-qPCR, qPCR and western blot. METTL3 depletion decreased the stability of SLC7A11 mRNA, and IGF2BP2 as m6A reader was involved in this process. Moreover, METTL3 knockdown attenuated the binding between SLC7A11 mRNA and IGF2BP2, finally leading to accelerate SLC7A11 mRNA degradation. Triptolide inhibited METTL3-mediated SLC7A11 expression, thus suppressing malignancy of OSCC cells. In conclusion, the new finding of the manuscript is that METTL3 enhances the mRNA stability of SLC7A11 via m6A-mediated binding of IGF2BP2, which thus promotes OSCC progression, and triptolide inhibits OSCC by suppressing METTL3-SLC7A11 axis. Triptolide has a potential to be as an effective anti-OSCC drug targeted to METTL3.

Keywords: Oral squamous cell carcinoma, N6-methyladenosine, METTL3, IGF2BP2, SLC7A11, Triptolide

Introduction

Oral squamous cell carcinoma (OSCC) is the most common malignant tumor in head and neck region [1]. Despite of the progress in comprehensive treatments, the 5-year survival of OSCC patients remains dim [2]. Advanced OSCC commonly present poor prognosis, characterized by uncontrollable proliferation and aggressive lymphatic metastasis. As the molecular mechanisms underlying OSCC pathogenesis have not yet been completely understood, it is of pivotal urgency to develop novel biomarker as potent prognostic indicator and effective therapeutic target for patients.

RNA modification, as emerging hotspot of epitranscriptome in past decades, draws increas-

ing attention in fundamental research of tumor pathogenesis and translational medicine [3]. N6-methyladenosine (m⁶A), methylated adenosine at the N6 position, is the most abundant modification in mRNA and ncRNAs of eukaryotic species [4, 5], which functions throughout RNA fate from RNA transcription, decay, to translation [6]. Well-organized m⁶A RNA methylation is ubiquitously involved in diverse physiological processes [7-9], while abnormal m⁶A modification leads to a variety of diseases, including cancers [10].

METTL3, as the core catalytic subunit of m⁶A RNA methylation, was reported to serve as oncogene in many tumors, such as acute myeloid leukemia [11], non-small cell lung cancer [12], and hepatocellular carcinoma [13], while in other malignancies METTL3 could perform as a tumor suppressor [14, 15]. In OSCC, Liu et al. [16] revealed that METTL3 promotes tumorigenesis and metastasis through BMI1 m⁶A methylation, which paved the way for deep exploration on the mechanisms of METTL3 in OSCC progression. However, it requires further efforts to make it clear how METTL3 works in OSCC carcinogenesis and metastasis.

In this study, we investigated the function and underlying mechanism of METTL3 in the development of OSCC. Transcriptome sequencing and meRIP-qPCR were applied to identify the m⁶A modified target of METTL3, and METTL3 was found to play a potent role in SLC7A11 expression and post-translational modification. We aimed to explore a novel epigenetic cause of OSCC and evaluate the potential value of METTL3 as a promising diagnostic and therapeutic target.

Materials and methods

Patients and samples

94 OSCC patients who underwent surgical treatment at the Peking University School and Hospital of Stomatology (PKU-SS) in 2014 were enrolled. 13 pairs of OSCC tumor and adjacent normal tissues were collected in PKU-SS, which were immediately frozen in liquid nitrogen and stored at -80°C. No patient had received local or systemic treatment before operation. Informed consent was obtained from all patients. This study was approved by the Ethics Committee of Peking University School and Hospital of Stomatology (NO. PK-USSIRB-202053004).

Immunohistochemistry

The tissue sections were collected, deparaffinized and rehydrated, followed by antigen retrieval. Then, the samples were incubated with anti-METTL3 antibody (Abcam, UK) overnight at 4°C. All images were captured with an optimal microscope (Olympus). The staining immunoscore was calculated by multiplying the proportion score and the intensity score [17].

Cell culture and treatment

The human OSCC cell lines CAL27 was obtained from American Type Culture Collection (ATCC, CRL-2095) and WSU-HN6 was obtained from central laboratory of Peking University School and Hospital of Stomatology. The cells were cultured in DMEM (Gibco, USA) containing 10% FBS (Sigma, USA) and 1% penicillin/streptomycin in a 37°C incubator with 5% CO_2. Triptolide was obtained from MedChemExpress (USA), and added into complete DMEM at 0, 10, 30 and 50 nM for further detection.

The siRNA targeting METTL3 (Ruibo Biosciences, China) and IGF2BP2, SLC7A11 overexpression plasmid (Hanbio Biotechnology, China) were transfected using the JetPrimer (Polyplus transfection, France). Lentivirus containing METTL3 shRNA (Hanbio Biotechnology, China) was used to construct a stable METTL3 knockdown cell line. The indicated sequences of siRNA and shRNA are listed in Table S1.

Dot blot assay

After transfection by siRNA for 24 h, the mRNA was purified by Dynabeads™ mRNA DIRECT™ Purification Kit (Thermo, USA). Then, the purified mRNA (400 ng) was spotted onto a nylon membrane (GE Healthcare, USA) and then crosslinked by UV. The nylon membrane was incubated with m⁶A antibody (Abcam, UK) overnight. The dot blots were visualized by ECL detection. For the control, the spotted mRNA was stained with methylene blue.

Quantification of the m⁶A modification

The global m⁶A level of mRNA was measured by an m⁶A-RNA methylation quantification kit (Abcam, UK), following the manufacturer's protocol. The m⁶A levels were colorimetrically quantified by reading the absorbance at a wavelength of 450 nm by a microplate reader (Thermo Fisher Scientific, USA).

Western blot

After transfection by siRNA for 48 h, total proteins were extracted from the cells using RIPA buffer (Huaxingbio, China) containing a protease inhibitor and phosphatase inhibitors. The protein was separated using SDS-PAGE and then transferred to PVDF membranes (BioRad, USA). Thereafter, the membranes were blocked and incubated with primary antibodies (Table S2) at 4°C overnight. The membranes were visualized using an ECL detection reagent (Cwbiotech, China).

qPCR

After transfection by siRNA for 24 h, total RNA from WSU-HN6 or CAL27 cells was extracted using TRIzol reagent (Ambion, USA) according to the product's protocol. The cDNA was synthesized using a reverse transcription kit (Promega, Madison, WI, USA). qPCR assays were performed using SYBR Green (Roche, Switzerland) in an ABI 7500 Real-Time PCR Detection System (Applied Biosystems). GAPDH was used as the endogenous control. The primer sequences are shown in Table S3.

Cell proliferation assays

Cell Counting Kit-8 (CCK-8) (Dojindo, Japan) was performed as the manufacturer's protocol. After treatment, CCK-8 solution was added and the absorbance at 450 nm was recorded using a microplate reader (Thermo Fisher Scientific, USA). Ki-67 flow cytometry analysis was applied after 48 h transfection. The transfected cells were collected and incubated with Ki-67 antibody (Biolegend, USA) in dark for 30 min. Analysis was performed by using a flow cytometer (DxP Athena, Cytexbio).

Wound healing assay

After treatment, the cells were scratched with pipette tips. Images were taken at the indicated time with an optimal microscope and analyzed using ImageJ 1.52K software. For CAL27, the indicated time was 30 h, while for WSU-HN6, it was 8 h.

Invasion transwell assay

After treatment, the cells were transferred to the transwell chambers (Millipore, Germany). At indicated time, the chambers were stained with 0.1% crystal violet (Solarbio, China). The imaged were obtained with an optimal microscope and analyzed using ImageJ 1.52K software. For CAL27, the indicated time was 30 h, while for WSU-HN6, it was 8 h.

MeRIP and transcriptome sequencing

MeRIP and transcriptome sequencing was performed by Cloudseq Biotech Inc. (Shanghai, China). GO and KEGG enrichment analysis were performed on DAVID 6.8 website (https://david.ncifcrf.gov/) for the differentially methylated genes. The read alignments on genome could be visualized using the popular tool IGV.

RNA stability detection

To detect the RNA stability in CAL27 and WSU-HN6 cells, actinomycin D (Act-D; 10 µg/mL; Sigma, USA) was administrated to cells. At the indicated time point of 3 h and 6 h after Act-D treatment, SLC7A11 mRNA expression was detected as described before.

RIP-qPCR

RIP assays were performed by Imprint® RNA Immunoprecipitation (RIP) Kit (Sigma, USA) as the manufacturer's protocol. The immunoprecipitation antibodies of m^6A, IGF2BP2 and IGF2BP3 were obtained from Abcam as shown in Table S2. mRNA expression was detected as described before.

Animal experiments

Female BALB/c nude mice (4 weeks old, weighted 18-22 g) were purchased from Beijing Vital River Laboratory Animal Technology. All animal studies were performed in compliance with the regulations and the Peking University institutional animal care guidelines and conducted according to the AAALAC and the IACUC guidelines (NO. LA2019011).

Establishment and analysis of subcutaneous xenograft tumor model and orthodontic xenograft tumor model was performed as we described before [18, 19]. In brief, in subcutaneous xenograft tumor model, 1×10^6 WSU-HN6 cells were injected subcutaneously into BALB/c nude mice. Tumor width and length were recorded every 2 days by the following formula: volume = (length × width^2)/2. When the tumor sizes were above 50 mm^3, vector (0.1% DMSO diluted in sterilized PBS) and triptolide (0.5 mg/kg weight) were intraperitoneally

injected into each mouse every 2 days. The tumor weight was detected after the mice were sacrificed. In orthodontic xenograft tumor model, $1×10^6$ WSU-HN6 cells were injected into the right side of the anterior third of the tongue. A nutritious semi-liquid diet was provided since 15th day after inoculation, to alleviate weight loss due to tumor growth in the tongue. At 6 days after inoculation, vehicle (0.1% DMSO diluted in sterilized PBS) and triptolide (0.5 mg/kg weight) were intraperitoneally injected into each mouse every 2 days. At 20 days after inoculation, the mice were detected by living imaging system to detect metastasis and the lymph nodes were collected and processed for histology and immunohistochemistry.

Statistical analysis

The Mann-Whitney U test was used to analyze the relationship between METTL3 expression and T or N stages in patients with OSCC. The Chi-square test was used to analyze the relationship between METTL3 expression and the clinical parameters of the patients. The Kaplan-Meier method was used for survival analysis. Student *t*-tests were used to compare the difference between two groups. A *P* value of <0.05 was considered significantly different. In addition, all statistical analyses were performed using SPSS 22.0 for Windows. Results are expressed as mean ± SD.

Results

Increased m⁶A level in OSCC

To investigate the role of m^6A modification in OSCC, we detected m^6A level in 13 pairs of human OSCC samples and adjacent normal tissues by using the colorimetric m^6A quantification assay. Results showed that the m^6A levels in tumor tissues were significantly increased compared to that in their corresponding adjacent tissues (**Figure 1A**).

METTL3 is highly expressed in OSCC and associated with poor prognosis

By analyzing OSCC dataset in TCGA repository, we found that the methyltransferases were significantly higher in OSCC tissues than in adjacent normal tissues, especially METTL3 (P<0.0001), while demethylases ALKBH5 and FTO had no differences between tumor and normal tissues (**Figure 1B**), and the upregula-

tion of METTL3 expression in OSCC tissues was verified by qPCR analysis and IHC (**Figure 1C**, **1E**). Moreover, the m^6A level of total RNA in OSCC tissues was positively correlated with METTL3 expression (**Figure 1D**). We evenly separated 330 OSCC patients of TCGA cohort into METTL3 high-expressed group and low-expressed group based on the median of METTL3, and analyzed the differential expressed genes. The GO and KEGG analyses of these differential expressed genes showed that proliferation and migration associated biological processes (**Figure 1F**), as well as cell cycle, spliceosome, DNA replication and adherens junction pathways (**Figure 1G**) were aberrantly activated in METTL3 high-expressed OSCC group. To further explore the association between the expression of METTL3 and the clinical characters of OSCC, 94 OSCC samples were collected and analyzed by immunochemical method [17]. We identified the staining intensity of OSCC samples as showed in Figure S1, and the results indicated that OSCC patients with elevated expression of METTL3 had poor overall survival (**Figure 1H**), and suffered tumors with higher T stages (**Figure 1I**) and lymphatic metastatic rate (**Figure 1J**), while the other clinical characters, such as age, gender, clinical stage and pathological grading, presented few statistical differences (**Table 1**).

Knockdown of METTL3 inhibited cell proliferation, migration and invasion of OSCC

To explore the effects of METTL3 on tumor progression, we firstly investigated whether METTL3 suppression was associated with cell proliferation, migration and invasion *in vitro*. METTL3 suppression mediated by siRNA was assessed in CAL27 and WSU-HN6 cells. As shown in **Figure 2A-C**, both expression and function of METTL3 were dramatically inhibited in siMETTL3 groups. The CCK8 assay and Ki67 detection suggested that suppression of METTL3 slowed down the proliferation of OSCC cells (**Figure 2D**, **2E**). The invasion transwell assay results revealed the reduction of invasive ability in the cells of test group compared to that in the control group (**Figure 2F**). The wound healing assay results showed that cells transfected with siMETTL3 had slower migration than the control group (**Figure 2G**). Given that siMETTL3#1 showed a stronger inhibition on malignance of OSCC cells, it was used to further perform rescue assays and explore the
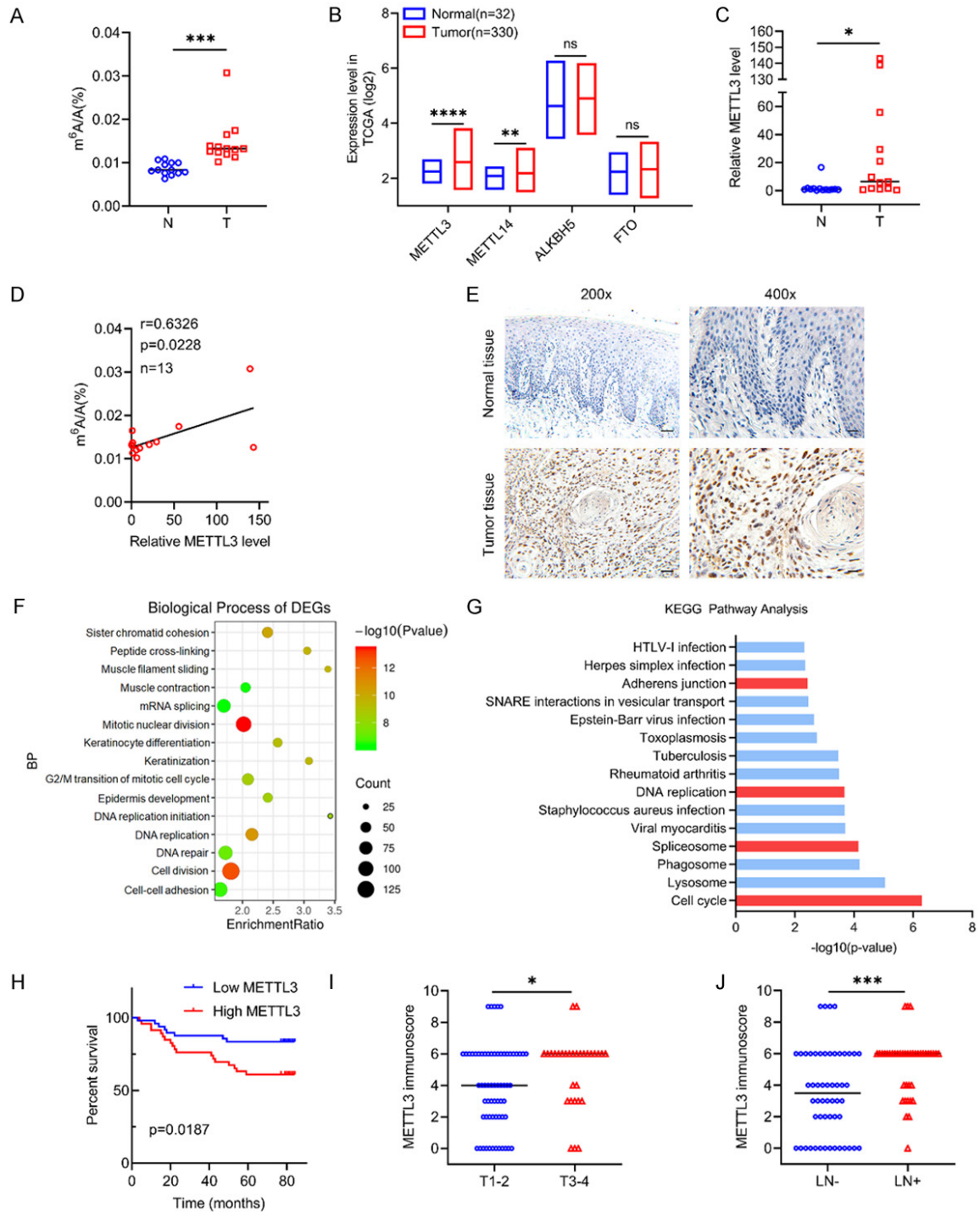
Figure 1. METTL3 is highly expressed in OSCC and associated with poor prognosis. A. m⁶A modification was detected using m⁶A colorimetric quantification in 13 pairs of OSCC tumor and adjacent normal tissues. B. Catalytic proteins involved in m⁶A modification were assessed in TCGA OSCC cohort (blue box for normal tissues, n=32; red box for tumor tissues, n=330). C. Relative increased level of METTL3 was confirmed in the OSCC tumor and adjacent normal tissues by qPCR (n=13). D. Pearson correlation analysis between METTL3 expression and m⁶A modification level (n=13). E. Representative image of METTL3 immunohistochemical staining in OSCC tumor and normal oral mucosa tissues (200×, scale bar: 50 μm; 400×, scale bar: 20 μm). F, G. GO enrichment analysis and KEGG pathway analysis of the differential expressed genes derived from METTL3 high-expressed group and low-expressed group in TCGA OSCC cohort. H. Kaplan-Meier survival curves of OS based on METTL3 immunoscore in 94 OSCC patients. The log-rank test was used to calculate the significant level. I, J. The relationship between METTL3 expression and T stage, lymphatic metastasis of OSCC was analyzed by using the Mann-Whitney U test. "LN-" indicates no metastasis (n=54), while "LN+" indicates the presence of metastasis (n=40). Data are presented as means ± standard deviation (ns P>0.05, *P<0.05, **P<0.01, ***P<0.001, ****P<0.0001).

Table 1. The relationship between METTL3 expression and clinical characters of OSCC

	Total	METTL3 expression		P value
		Low	High	
Age				
≤55	33	19	14	0.353
>55	61	29	32	
Gender				
Male	51	24	27	0.398
Female	43	24	19	
Pathological grading				
I	37	18	19	0.706
II-III	57	30	27	
Clinical stage				
I-II	53	31	22	0.101
III-IV	41	17	24	
T stage				
1-2	64	38	26	0.019*
3-4	30	10	20	
Lymphatic metastasis				
No	54	36	18	<0.001***
Yes	40	12	28	

*P<0.05, ***P<0.001.

mechanisms of METTL3. Moreover, a stable METTL3 knockdown cell line was constructed to further validate the alterations of phenotypes of OSCC cells (**Figure 3A-C**). Consistently with above *in vitro results*, shMETTL3 cells demonstrated suppressed growing, migration and invasive (**Figure 3D-F**) ability compared to control cells. To test our *in vitro* findings, we established subcutaneous xenograft tumor model and orthodontic xenograft tumor model. Consistent with our *in vitro* observations, knockdown of METTL3 resulted in significant suppression of the tumor volume (**Figure 3G, 3H**) and tumor weight (**Figure 3I**). Besides, as shown in **Figure 3J**, significant lower lymphatic metastasis rate was observed in the shMETTL3 group (2/10, 20%) than the control group (10/10, 100%) by living imaging system (**Figure 3K**) and pan-CK IHC staining of lymph nodes (**Figure 3L**). Collectively, these results suggested the reversal of malignancy in OSCC cell lines in response to METTL3 knockdown.

METTL3 promotes OSCC progression by targeting SLC7A11 mRNA

To investigate the modified target by which METTL3 suppressed malignant phenotypes of

OSCC cells, we performed meRIP-sequencing and transcriptome sequencing. To verify the specific occurrence of m⁶A in transcripts in OSCC cells, m⁶A peaks distribution was analyzed. The results showed that the dominant sequence of m⁶A motifs was "RRACH" (**Figure 4A**), and further distribution analysis of m⁶A peaks, as shown in **Figure 4B**, revealed that m⁶A sites were most enriched in the CDS region (59.2% and 59.9% in siNC and siMETTL3 groups respectively). Of all m⁶A peaks, 3075 were upregulated, while 1446 were downregulated in METTL3-knockdown group (**Figure 4C**). GO enrichment analysis revealed that the differential m⁶A genes were primarily involved in the regulation of cell proliferation, cell migration and cell adhesion, i.e. (**Figure 4D**), and KEGG analysis suggested that suppression of METTL3 influenced many pathways involved in tumorigenesis, such as Wnt and Hippo signaling pathways (**Figure 4E**). To confirm the target gene of METTL3, we operated the screening as shown in **Figure 5A** and six candidate genes including ADM2, ALDH1L2, ASNS, LAT2, PSAT1 and SLC7A11 were screened by Venn analysis of meRIP-sequencing and transcriptome sequencing. Among them, the mRNA expression of SLC7A11 showed the significant shift after METTL3 knockdown in both OSCC cell lines (**Figure 5B, 5C**), while the other genes presented opposite changes or few significant differences. Western blot further verified the downregulated status of SLC7A11 mRNA after METTL3 depletion (**Figure 5D**). The IGV plot revealed that the m⁶A peak distribution on SLC7A11 mRNA was suppressed in siMETTL3 group (**Figure 5E**), and METTL3 knockdown remarkably reduced the m⁶A level of SLC7A11 mRNA in the two OSCC cell lines (**Figure 5F**). Furthermore, through overexpression of SLC7A11 (**Figure 5G, 5H**), the proliferation, migration and invasion abilities were restored partly in METTL3-knockdown OSCC cells (**Figure 5I-N**). These results suggested that SLC7A11 mRNA was the modified target of METTL3.

METTL3 enhances the SLC7A11 stability through an m⁶A-IGF2BP2 dependent manner

As shown in **Figure 5B-D**, knockdown of METTL3 resulted in a remarkable decrease at SLC7A11 expression level. Therefore, the sta-
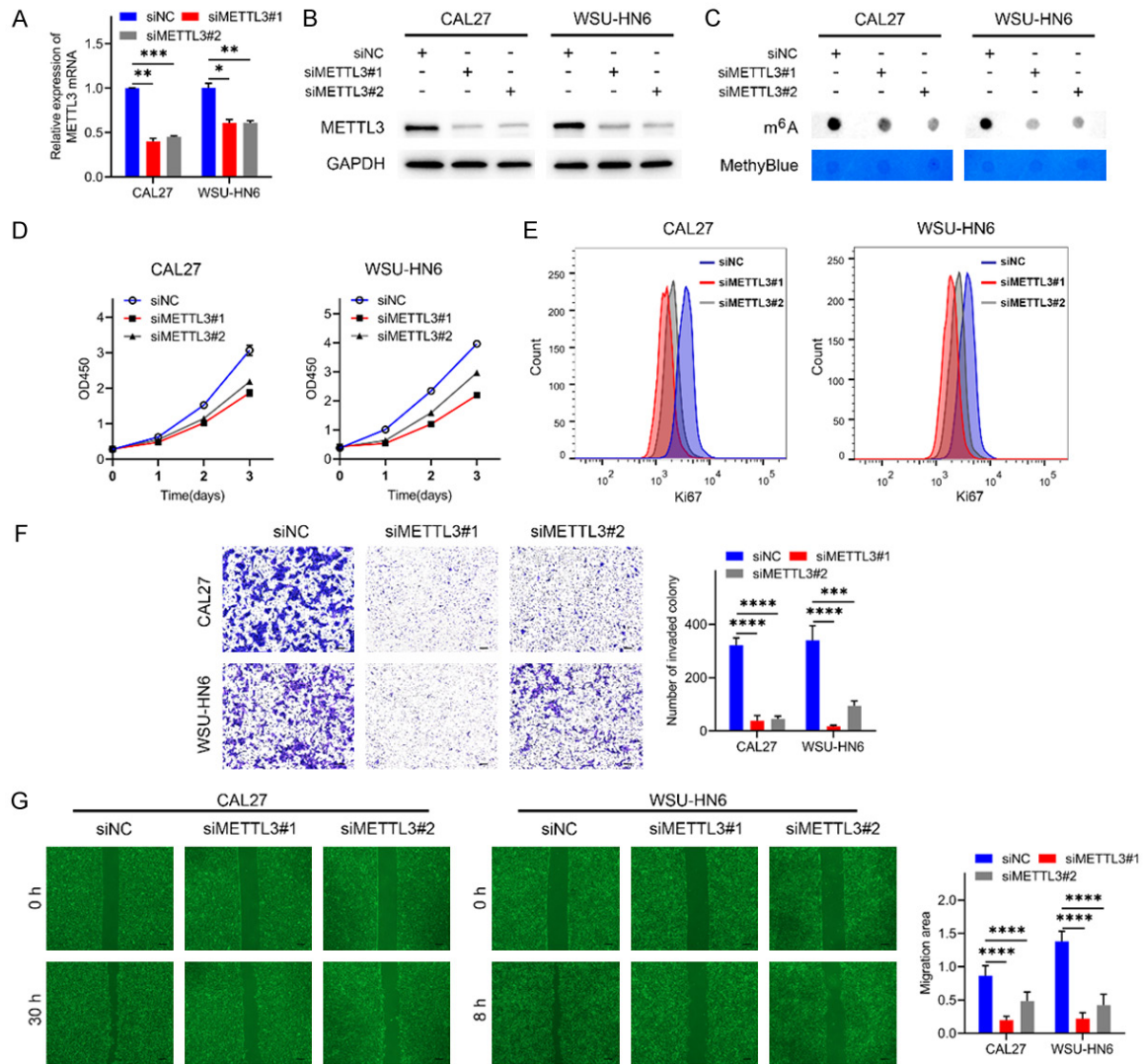
Figure 2. Knocking down the expression of METTL3 impaired the malignancy of OSCC cell lines. A, B. The two panels showed the expression level of METTL3 in CAL27 and WSU-HN6 transfected with siRNA determined by qPCR and western blot. C. Dot blot was performed to verify the suppressed m^{6}A level in OSCC cells after siRNA transfection. D, E. Effect of METTL3 depletion on proliferation activity by CCK8 and Ki67 assays. F. Effect of METTL3 depletion on transwell assay, representative graphs are shown (40×, scale bar: 200 μm). G. Effect of knocking down METTL3 level on wound healing assay, representative graphs are shown (40×, scale bar: 200 μm). Data are presented as means ± standard deviation (*P<0.05, **P<0.01, ***P<0.001, ****P<0.0001).

bility of SLC7A11 mRNA was detected to clarify whether METTL3 enhanced its expression by delayed RNA degradation. Indeed, SLC7A11 mRNA exhibited accelerated degradation after METTL3 depletion (**Figure 6A**, **6B**). To verify whether METTL3 strengthened the stability of target mRNA via an IGF2BP family-mediated m^{6}A-dependent manner, subsequently SLC7A-11 expression was detected by qPCR after silencing IGF2BP family. The results showed that inhibition of IGF2BP2 by siIGF2BP2#1/#2 significantly downregulated SLC7A11 level by

45.1%/41.7% and 68.7%/52.1%, and inhibition of IGF2BP3 by siIGF2BP3#1/#2 decreased SLC7A11 level by 38.4%/33.4% and 59.2%/49.6% in CAL27 and WSU-HN6 respectively (**Figure 6C**), while IGF2BP1 depletion by siIGF-2BP1#1/#2 slightly downregulated SLC7A11 expression (27.9%/4.2% and 27.5%/16.8% in CAL27 and WSU-HN6). Moreover, RIP-qPCR revealed that SLC7A11 mRNA bound strongly with IGF2BP2 (**Figure 6D**, 7.04%, 7.45% in CAL27 and WSU-HN6), while interacted weakly with IGF2BP3 (**Figure 6E**, 1.85%, 2.01% in
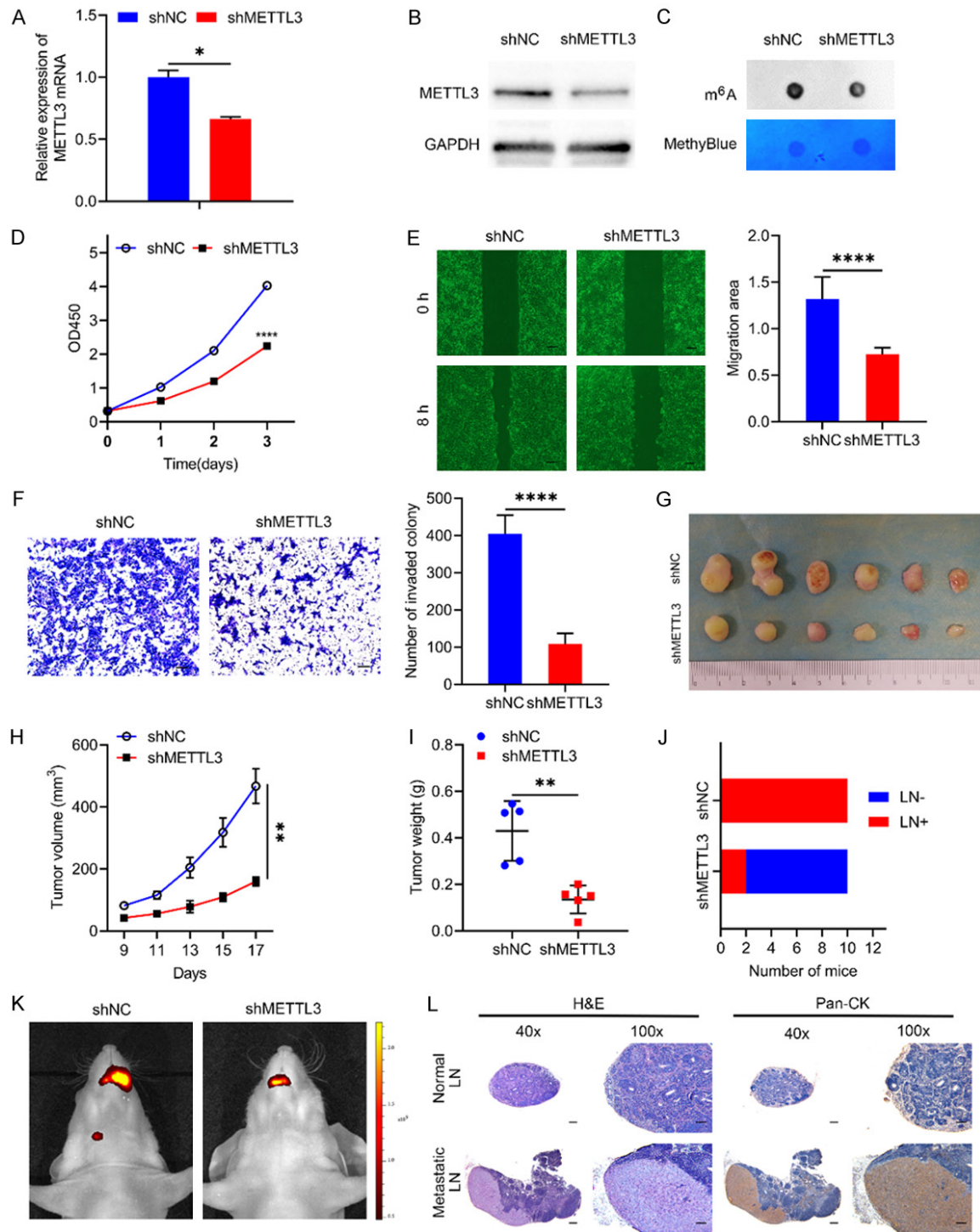
Figure 3. Stably knocking down METTL3 suppressed the malignancy of OSCC cells *in vitro* and *in vivo*. (A, B) The two panels showed the expression level of METTL3 in WSU-HN6 determined by qPCR and western blot after transfected with shMETTL3 lentivirus. (C) Dot blot was performed to verify the suppressed m^6A level in METTL3 stably depleted WSU-HN6. (D) Effect of METTL3 depletion on proliferation activity by CCK8 assay. (E) Effect of METTL3 depletion on wound healing assay, representative graphs are shown (40×, scale bar: 200 μm). (F) Effect of knocking down METTL3 level on transwell assay, representative graphs are shown (40×, scale bar: 200 μm). (G-I) Subcutaneous tumor models in nude mice showed the tumor growth rate (G, H) and tumor weights (I) at day 17 after the implantation of METTL3-knockdown and control WSU-HN6 cells (n=6 mice per group). (J) Orthodontic xenograft tumor model showed the lymphatic metastatic rate of METTL3-knockdown and control WSU-HN6 cells (n=10 mice per group). (K) Representative living imaging photos and (L) HE and pan-CK IHC photos of the lymph nodes with or without metastasis (40×, scale bar: 200 μm; 100×, scale bar: 100 μm). Data are presented as means ± standard deviation (*P<0.05, **P<0.01, ****P<0.0001).
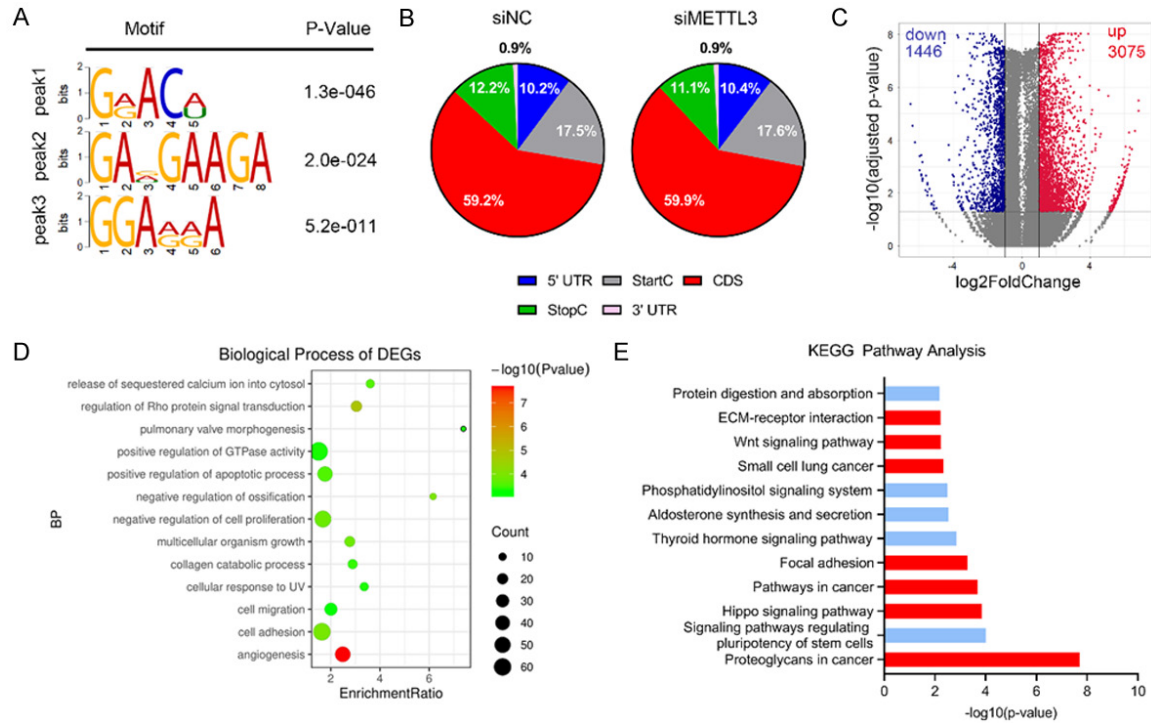
Figure 4. Analysis of the MeRIP-seq data of WSU-HN6 transfected with siMETTL3. A. Top sequence motif identified from MeRIP-seq peaks in control and METTL3-depleted cells. B. Distribution of m^{6}A peaks across all mRNAs in control and METTL3-depleted cells. C. Volcano plot of significantly altered m^{6}A peaks identified in MeRIP-seq in control and METTL3-depleted cells (FDR<0.05, fold change >2). D, E. GO enrichment analysis and KEGG pathway analysis of the differential m^{6}A peaks derived from comparison between control and METTL3-depleted cells.

CAL27 and WSU-HN6). Additionally, suppressed METTL3 expression attenuated the binding of SLC7A11 mRNA and IGF2BP2 by 69.3%, 50.1% compared to siNC groups in CAL27 and WSU-HN6 (**Figure 6F**). Therefore, these evidences supported that IGF2BP2 mediated the enhanced stability of SLC7A11 mRNA by METTL3 in an m^{6}A-dependent manner.

IGF2BP2 activation reversed the METTL3 knockdown-mediated degradation of SLC7A11 mRNA and inhibition of malignancy in OSCC

To investigate whether IGF2BP2 was a dominant contributor to the METTL3-SLC7A11 axis in OSCC progression, we evaluated whether IGF2BP2 activation could rescue the effects of METTL3 knockdown on the biological behaviors of OSCC cell lines. As shown in **Figure 7A-D**, overexpression of IGF2BP2 significantly reversed the inhibiting effects of silencing METTL3 on SLC7A11 expression and mRNA stability. Moreover, cell proliferation, invasion and migration were restored in METTL3-knockdown cells rescued with overexpressed IGF2-

BP2 (**Figure 7E-J**). Taken together, these findings suggested that overexpression of IGF2-BP2 rescued the METTL3 depletion-induced degradation of SLC7A11 mRNA and suppressed phenotypes of OSCC cells.

Triptolide inhibited cell proliferation, migration and invasion of OSCC via METTL3-SLC7A11 axis

To explore the effects of triptolide on METTL3 in OSCC cells, we firstly detected the METTL3-SLC7A11 expression in triptolide-treated group. As shown in **Figure 8A**, **8B**, both transcriptional and protein expression of METTL3 and SLC7A11 were dramatically inhibited by triptolide in a dose-dependent manner. The CCK8 assay and Ki67 detection suggested that 30 nM triptolide slowed down the proliferation of OSCC cells (**Figure 8C**, **8D**). The wound healing assay results showed that cells treated with 30 nM triptolide migrated slower than the vehicle (**Figure 8E**). The invasion transwell assay results revealed the reduction of invasive ability in the cells of test group compared to that in
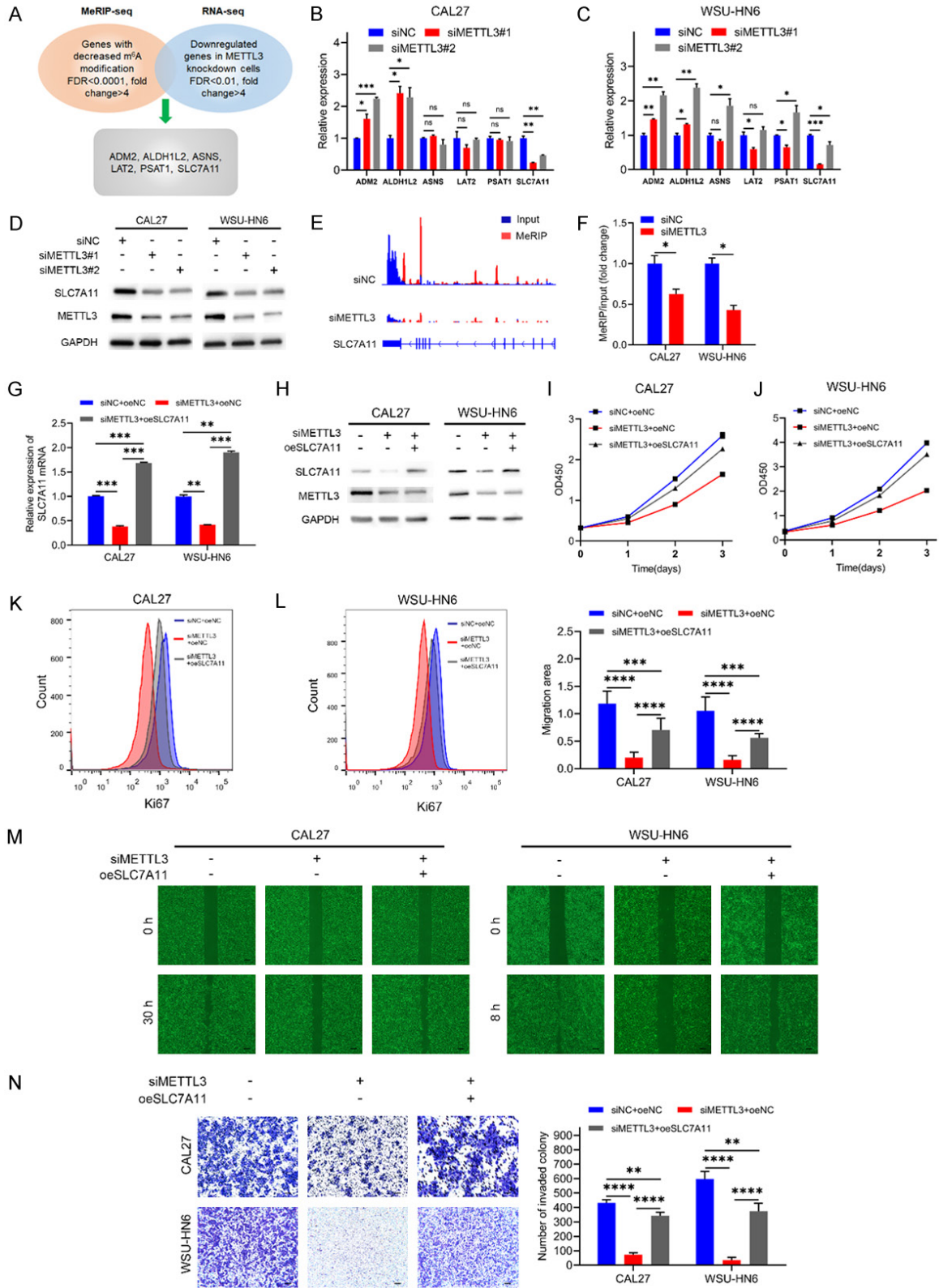
Figure 5. METTL3 promotes OSCC progression by targeting SLC7A11 mRNA. A. The flow chart for selected candidate target genes of METTL3 in WSU-HN6 METTL3 depletion cells is shown. B, C. qPCR analysis of alterations in the six candidate target genes in control and METTL3-knockdown OSCC cells. D. Verification of SLC7A11 expression in OSCC cells transfected with siRNA by western blot. E. The relative abundance of m⁶A sites along SLC7A11 mRNA

in control and METTL3-knockdown WSU-HN6 cells, as shown in IGV diagram. F. The altered m⁶A modification level of SLC7A11 mRNA in OSCC cells transfected with siMETTL3. G, H. The two panels showed the expression level of SLC7A11 in METTL3-knockdown OSCC cells with SLC7A11 activation determined by qRT-PCR and western blot. I-L. Effect of SLC7A11 rescue on proliferation activity of METTL3-knockdown OSCC cells by CCK8 and Ki67 assays. M. Effect of overexpressed SLC7A11 on wound healing assay of METTL3-knockdown OSCC cells, representative graphs are shown (40×, scale bar: 200 μm). N. Effect of SLC7A11 rescues on transwell assay of METTL3-knockdown OSCC cells, representative graphs are shown (40×, scale bar: 200 μm). Data are presented as means ± standard deviation (ns P>0.05, *P<0.05, **P<0.01, ***P<0.001, ****P<0.0001).
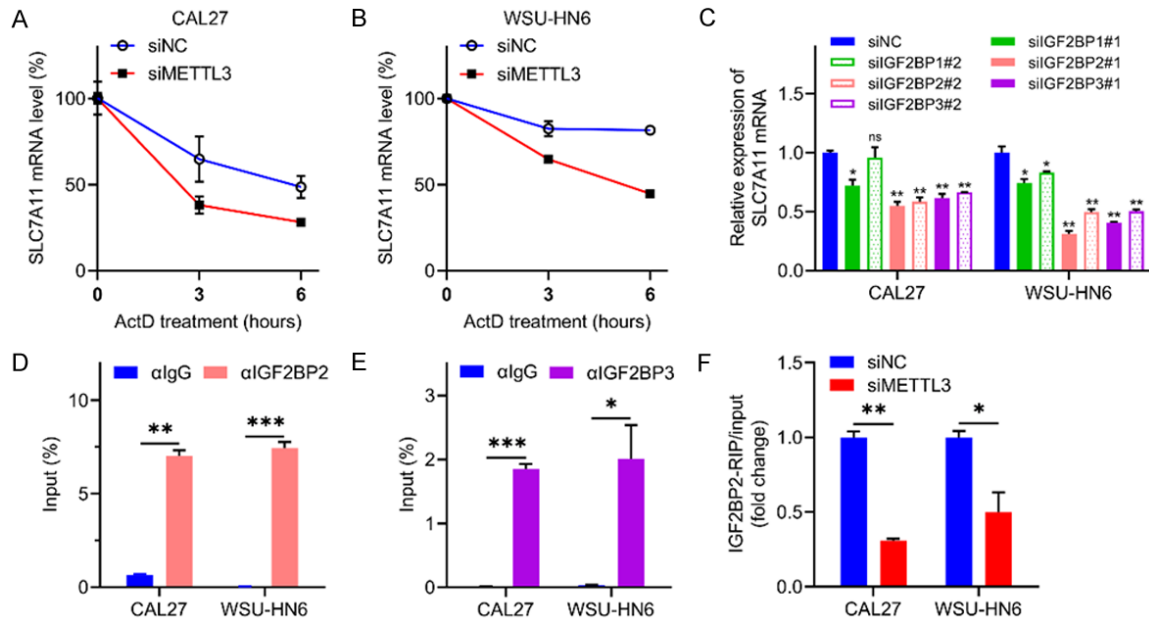
Figure 6. METTL3 enhanced SLC7A11 mRNA stability via m⁶A-mediated IGF2BP2 binding. A, B. The degradation rate of SLC7A11 mRNA at the indicated times after actinomycin D (5 μg/ml) treatment in CAL27 and WSU-HN6 cells after METTL3 inhibition. C. The relative expression of SLC7A11 in OSCC cells after inhibition of IGF2BP family respectively. D, E. RIP-qPCR showed the binding strength between SLC7A11 mRNA and IGF2BP2 as well as IGF2BP3. F. IGF2BP2 RIP-qRT-PCR presented the alteration of binding proportion between SLC7A11 mRNA and IGF2BP2. Data are presented as means ± standard deviation (ns P>0.05, *P<0.05, **P<0.01, ***P<0.001).

the control group (**Figure 8F**). *In vivo* studies revealed that triptolide caused significant suppression of the tumor volume (**Figure 8G**, **8H**) and tumor weight (**Figure 8I**). Besides, as shown in **Figure 8J**, significant lower lymphatic metastasis rate was observed in the triptolide group (2/7, 29%) than the control group (7/7, 100%).

Discussion

The first new finding of the study is that METTL3 regulates SLC7A11 expression in a novel m⁶A-mediated manner, finally leading to OSCC progression, which indicates METTL3 can serve as a promising biomarker for OSCC prognosis.

Many recent studies have partly revealed the underlying mechanisms of m⁶A modification in cancers. Thereinto, METTL3 presents a double-edged sword effect in a significant tumor-specific manner [4]. A latest study has uncovered the effects of m⁶A methylation on OSCC stemness by modifying BMI1 [16]. However, the exact roles of m⁶A methylation in OSCC carcinogenesis and metastasis remain poorly defined. In the present research, we verified the upregulation of METTL3 in OSCC tissues, and METTL3 was further found to serve as a formidable prognostic factor of aggressive tumor growth and lymphatic metastasis in OSCC. Functional trials indicated that METTL3 could promote the proliferation and lymphatic metastasis of OSCC cells *in vitro* and *in vivo*. These results suggested that METTL3 is a potent prognostic factor which plays critical roles in OSCC progression.
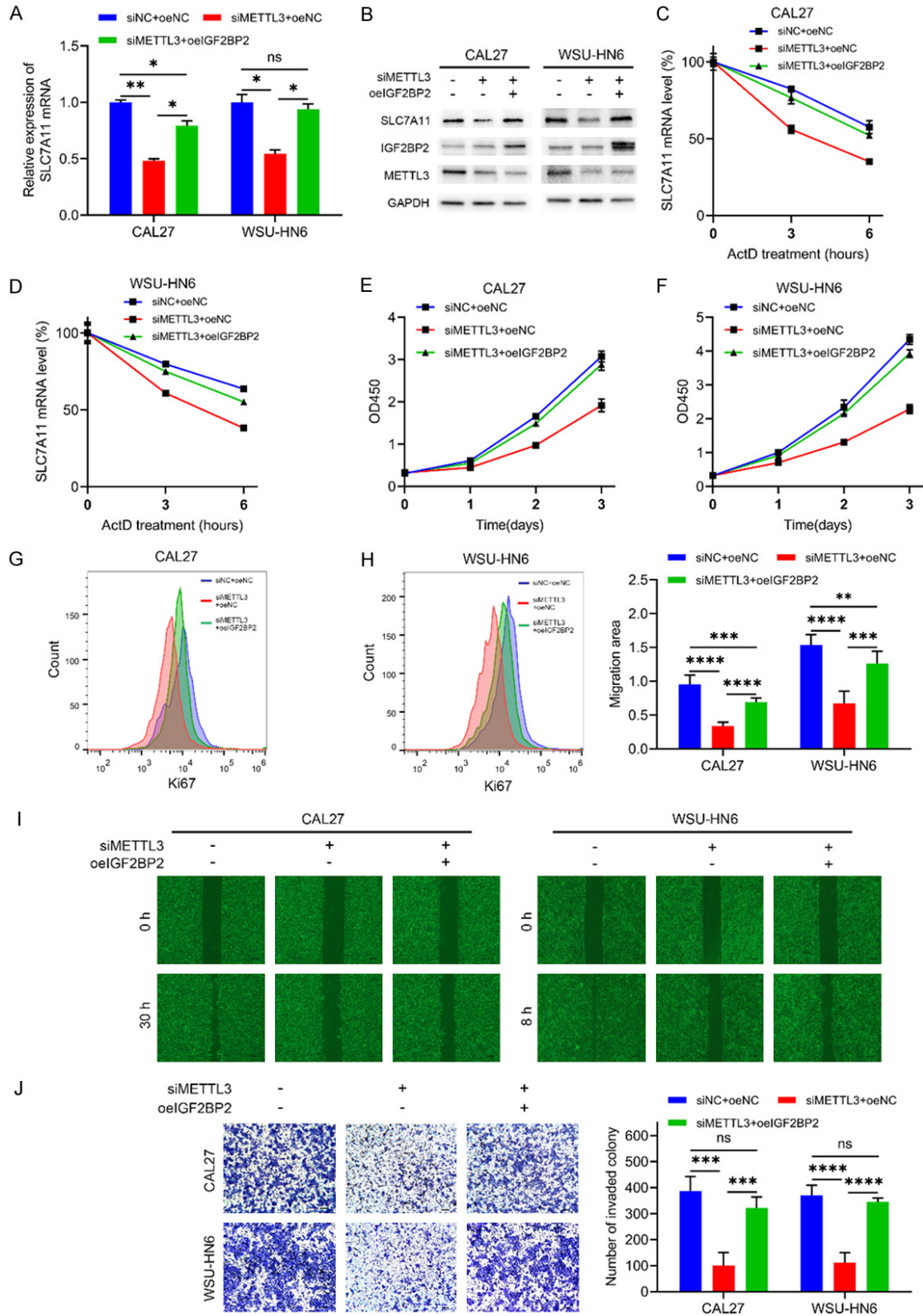
Figure 7. IGF2BP2 reversed the METTL3 knockdown-mediated degradation of SLC7A11 mRNA and inhibition of malignancy in OSCC. A, B. The two panels showed the expression level of SLC7A11 in METTL3-knockdown OSCC cells with IGF2BP2 activation determined by qRT-PCR and western blot. C, D. The degradation rate of SLC7A11 mRNA at

the indicated times after actinomycin D (5 µg/ml) treatment in METTL3-knockdown OSCC cells with IGF2BP2 activation. E-H. Effect of IGF2BP2 rescue on proliferation activity of METTL3-knockdown OSCC cells by CCK8 and Ki67 assays. I. Effect of IGF2BP2 rescues on transwell assay of METTL3-knockdown OSCC cells, representative graphs are shown (40×, scale bar: 200 µm). J. Effect of overexpressed IGF2BP2 on wound healing assay of METTL3-knockdown OSCC cells, representative graphs are shown (40×, scale bar: 200 µm). Data are presented as means ± standard deviation (ns P>0.05, *P<0.05, **P<0.01, ***P<0.001, ****P<0.0001).
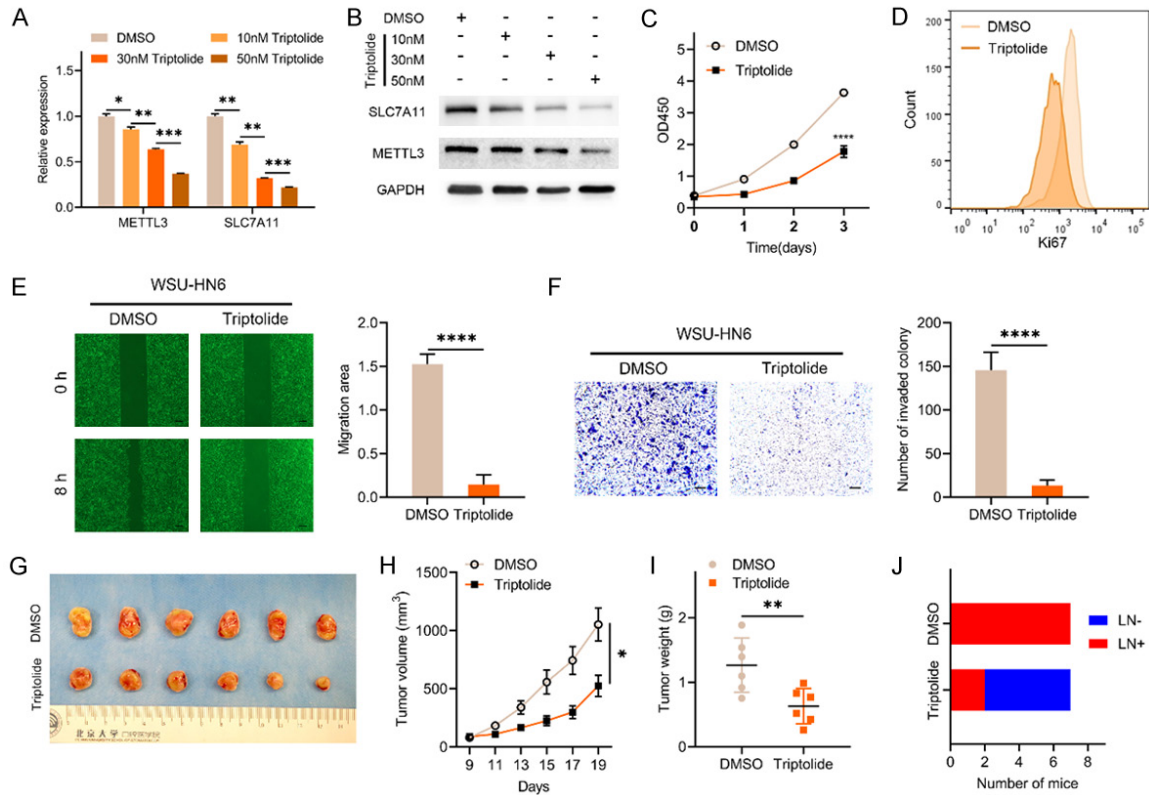
Figure 8. Triptolide impaired the malignancy of OSCC cell lines via METTL3-SLC7A11 axis. (A, B) The two panels showed the expression level of METTL3 and SLC7A11 in WSU-HN6 treated with triptolide by qPCR and western blot. (C, D) Effect of triptolide on proliferation activity by CCK8 and Ki67 assays. (E) Effect of triptolide on wound healing assay, representative graphs are shown (40×, scale bar: 200 µm). (F) Effect of triptolide on transwell assay, representative graphs are shown (40×, scale bar: 200 µm). (G-I) Subcutaneous tumor models in nude mice showed the tumor growth rate (G, H) and tumor weights (I) of WSU-HN6 cells (n=6 mice per group). (J) Orthodontic xenograft tumor model showed the lymphatic metastatic rate of triptolide treated and control WSU-HN6 cells (n=7 mice per group). Data are presented as means ± standard deviation (*P<0.05, **P<0.01, ***P<0.001, ****P<0.0001).

As the pivotal catalytically active subunit of m6A methyltransferase complex (MTC) [20-22], METTL3 forms the majority of m6A deposition on mRNA. Indeed, we identified that m6A modification level was positively correlated with the METTL3 expression in OSCC tissues, which was consistent with the m6A methylated effect of METTL3. RNA methyltransferase METTL3 may participate in regulating the mRNA stability through m6A modification of target genes [23]. However, the underlying modification targets of METTL3-regulated genes in OSCC remain unclear. Our transcriptome-wide m6A-seq assay

showed that METTL3 depletion induced m6A alteration was involved in cancer proliferation and metastasis associated functions, further confirming the pro-tumoral role of METTL3 in OSCC. Then the combined analysis of sequencing data and subsequent validation and functional studies suggested that METTL3 upregulated SLC7A11 expression via enhanced mRNA stability mediated by m6A-IGF2BP2 dependent manner.

Based on previous studies, SLC7A11 expression is regulated in three manners: (i) transcrip-

tional factors, including ATF4 [24], NRF2 [25] and p53 [26], (ii) epigenetic regulation, such as histone 2A mono-ubiquitination [27], (iii) post-translational regulation by nonsense-mediated mRNA decay [28] and microRNAs [29]. In this work, we firstly reported a novel regulatory mechanism of SLC7A11 by METTL3-mediated m[6]A RNA methylation. We found that knock-down of METTL3 downregulated SLC7A11 in an m[6]A-dependent way. Further functional assays determined the underlying regulatory mechanism of METTL3 on SLC7A11 was mediated by enhanced mRNA stability. IGF2BP family was reported to fortify the stability of their target mRNAs in an m[6]A-dependent manner and therefore affect gene expression output [30]. Consistently, we found SLC7A11 mRNA preferred to bind with IGF2BP2, and METTL3 depletion attenuated the binding between IGF2BP2 and SLC7A11 mRNA. Collectively, METTL3 enhances the SLC7A11 stability through an m[6]A-IGF2BP2 dependent manner.

In OSCC, previous studies have revealed that SLC7A11 works as oncogene in tumorigenesis. For example, cisplatin treatment could induce SLC7A11 expression, thus promoting cisplatin chemoresistance in OSCC cells, and SLC7A11 inhibition sensitized OSCC cells to cisplatin [31]. Overexpression of SLC7A11 was associated with advanced T classification and lympho-vascular invasion, and multivariate analysis indicated that high expression of SLC7A11 was independent predictors of poor prognosis [32]. These findings support the underlying mechanism that enhanced RNA stability of SLC7A11 mediated by METTL3-m[6]A-IGF2BP2 axis promotes OSCC progression. Thus, targeting both METTL3 and SLC7A11 can be a potential strategy for OSCC treatment.

The second new finding of the study is that triptolide could suppress OSCC cells through regulating METTL3-SLC7A11 axis, which indicates METTL3-SLC7A11 axis can serve as a promising target for OSCC treatment. DAA, a chemical inhibitor of the internal S-adenosylhomocysteine hydrolase, is the widely used m[6]A inhibitor, and we found it is effective to inhibit the proliferation and metastatic abilities of OSCC cells (data not shown). Though DAA showed potent suppression on OSCC malignancy, it could obviously weaken the physical condition of tumor-bearing nude mice after three-day intraperitoneal injection. Given the strong side effects of DAA, a more specific inhibitor of

METTL3 or its target genes needs to be developed for OSCC patients. Especially for those OSCC patients with higher METTL3 expression treatment, as our results showing, SLC7A11-targeted treatment can be applied to impair OSCC progression. To explore a drug which can potentially regulate the METTL3-SLC7A11 axis, we reviewed previous studies about anti-tumor materials which targeted at SLC7A11 with unclear mechanisms. Then, we found that triptolide, a diterpenoid epoxide from tripterygium wilfordii, effectively inhibited SLC7A11 expression in IDH1 mutated glioma cells [33]. However, the underlying regulatory ways of triptolide on SLC7A11 remained little known. Accordingly, we applied triptolide to treat OSCC cells, and the results showed a dose-dependent inhibition on both METTL3 and SLC7A11 expression after triptolide treatment. Furthermore, triptolide exhibited strong inhibitory effects on proliferation and metastatic abilities of OSCC cells. These results indicated that triptolide inhibited cell proliferation, migration and invasion of OSCC via METTL3-SLC7A11 axis. Previous studies have established a critical role of SLC7A11-mediated cystine uptake in suppressing ferroptosis and maintaining cancer progression under oxidative stress conditions [34]. Thus, our finding may provide a promising therapeutical strategy for OSCC patients with higher METTL3 expression by applying treatment targeting ferroptosis, such as triptolide.

In conclusion, as shown in **Figure 9**, we find the new epigenetic regulation METTL3-IGF2BP2-SLC7A11 axis. Suppression of METTL3 blocks proliferation and lymphatic metastasis in OSCC cell lines and mouse xenograft model, which indicates that targeting METTL3 in cancer cells could be an effective therapeutic strategy. Triptolide exerts anti-tumor effects in OSCC cells through regulating METTL3-SLC7A11 axis, which further confirms the therapeutic significance of targeting METTL3. Taken together, our findings set new light into the critical role of METTL3 in OSCC development, and indicate the novel significance of the molecular mechanism of m[6]A epitranscriptomic modification in cancer research.
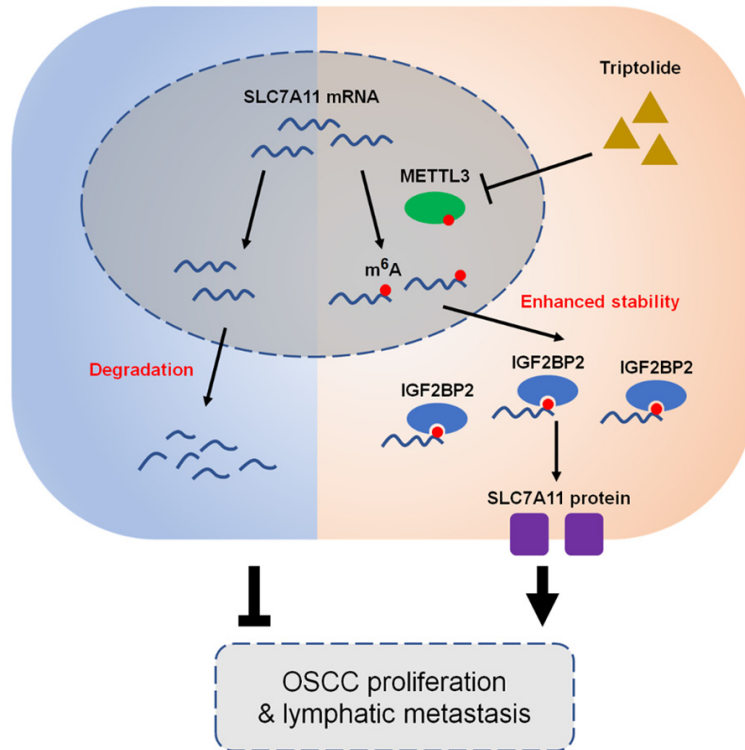
Figure 9. Schematic model of the epitranscriptomic regulation underlying the METTL3-SLC7A11 pathway.

Disclosure of conflict of interest

None.

Address correspondence to: Chuanbin Guo and Na Ge, Department of Oral and Maxillofacial Surgery, Peking University School and Hospital of Stomatology & National Center of Stomatology & National Clinical Research Center for Oral Diseases & National Engineering Laboratory for Digital and Material Technology of Stomatology & Beijing Key Laboratory of Digital Stomatology & Research Center of Engineering and Technology for Com-

puterized Dentistry Ministry of Health & NMPA Key Laboratory for Dental Materials, No. 22, Zhongguancun South Avenue, Haidian District, Beijing 100081, PR China. Tel: +86-010-8219-5295; E-mail: guodazuo@sina.com (CBG); jen_gena@126.com (NG); Yixiang Wang, Central Laboratory, Peking University School and Hospital of Stomatology, No. 22, Zhongguancun South Avenue, Haidian District, Beijing 100081, PR China. Tel: +86-010-82195295; E-mail: kqwangyx@bjmu.edu.cn

References

[1] Bray F, Ferlay J, Soerjomataram I, Siegel RL, Torre LA and Jemal A. Global cancer statistics 2018: GLOBOCAN estimates of incidence and mortality worldwide for 36 cancers in 185 countries. CA Cancer J Clin 2018; 68: 394-424.

[2] Chow LQM. Head and neck cancer. N Engl J Med 2020; 382: 60-72.

[3] Barbieri I and Kouzarides T. Role of RNA modifications in cancer. Nat Rev Cancer 2020; 20: 303-322.

[4] Huang H, Weng H and Chen J. m(6)A modification in coding and non-coding RNAs: roles and therapeutic implications in cancer. Cancer Cell 2020; 37: 270-288.

[5] Liu J, Li K, Cai J, Zhang M, Zhang X, Xiong X, Meng H, Xu X, Huang Z, Peng J, Fan J and Yi C. Landscape and regulation of m(6)A and m(6) Am methylome across human and mouse tissues. Mol Cell 2020; 77: 426-440, e426.

[6] Shi H, Chai P, Jia R and Fan X. Novel insight into the regulatory roles of diverse RNA modifications: re-defining the bridge between transcription and translation. Mol Cancer 2020; 19: 78.

[7] Mendel M, Chen KM, Homolka D, Gos P, Pandey RR, McCarthy AA and Pillai RS. Methylation of structured RNA by the m(6)A writer METTL16 is essential for mouse embryonic development. Mol Cell 2018; 71: 986-1000, e1011.

[8] Geula S, Moshitch-Moshkovitz S, Dominissini D, Mansour AA, Kol N, Salmon-Divon M, Hershkovitz V, Peer E, Mor N, Manor YS, Ben-Haim MS, Eyal E, Yunger S, Pinto Y, Jaitin DA, Viukov S, Rais Y, Krupalnik V, Chomsky E,

Zerbib M, Maza I, Rechavi Y, Massarwa R, Hanna S, Amit I, Levanon EY, Amariglio N, Stern-Ginossar N, Novershtern N, Rechavi G and Hanna JH. Stem cells. m6A mRNA methylation facilitates resolution of naive pluripotency toward differentiation. Science 2015; 347: 1002-1006.

[9] Xiang Y, Laurent B, Hsu CH, Nachtergaele S, Lu Z, Sheng W, Xu C, Chen H, Ouyang J, Wang S, Ling D, Hsu PH, Zou L, Jambhekar A, He C and Shi Y. RNA m(6)A methylation regulates the ultraviolet-induced DNA damage response. Nature 2017; 543: 573-576.

[10] He L, Li H, Wu A, Peng Y, Shu G and Yin G. Functions of N6-methyladenosine and its role in cancer. Mol Cancer 2019; 18: 176.

[11] Barbieri I, Tzelepis K, Pandolfini L, Shi J, Millán-Zambrano G, Robson SC, Aspris D, Migliori V, Bannister AJ, Han N, De Braekeleer E, Ponstingl H, Hendrick A, Vakoc CR, Vassiliou GS and Kouzarides T. Promoter-bound METTL3 maintains myeloid leukaemia by m(6)A-dependent translation control. Nature 2017; 552: 126-131.

[12] Jin D, Guo J, Wu Y, Du J, Yang L, Wang X, Di W, Hu B, An J, Kong L, Pan L and Su G. m(6)A mRNA methylation initiated by METTL3 directly promotes YAP translation and increases YAP activity by regulating the MALAT1-miR-1914-3p-YAP axis to induce NSCLC drug resistance and metastasis. J Hematol Oncol 2019; 12: 135.

[13] Chen M, Wei L, Law CT, Tsang FH, Shen J, Cheng CL, Tsang LH, Ho DW, Chiu DK, Lee JM, Wong CC, Ng IO and Wong CM. RNA N6-methyladenosine methyltransferase-like 3 promotes liver cancer progression through YTH-DF2-dependent posttranscriptional silencing of SOCS2. Hepatology 2018; 67: 2254-2270.

[14] Li X, Tang J, Huang W, Wang F, Li P, Qin C, Qin Z, Zou Q, Wei J, Hua L, Yang H and Wang Z. The m6A methyltransferase METTL3: acting as a tumor suppressor in renal cell carcinoma. Oncotarget 2017; 8: 96103-96116.

[15] Cui Q, Shi H, Ye P, Li L, Qu Q, Sun G, Sun G, Lu Z, Huang Y, Yang CG, Riggs AD, He C and Shi Y. m(6)A RNA methylation regulates the self-renewal and tumorigenesis of glioblastoma stem cells. Cell Rep 2017; 18: 2622-2634.

[16] Liu L, Wu Y, Li Q, Liang J, He Q, Zhao L, Chen J, Cheng M, Huang Z, Ren H, Chen J, Peng L, Gao F, Chen D and Wang A. METTL3 promotes tumorigenesis and metastasis through BMI1 m(6)A methylation in oral squamous cell carcinoma. Mol Ther 2020; 28: 2177-2190.

[17] Xiang G, Li X, Cao L, Zhu C, Dai Z, Pan S and Lin S. Frequent overexpression of PDK1 in primary nasopharyngeal carcinoma is associated with poor prognosis. Pathol Res Pract 2016; 212: 1102-1107.

[18] Wang Y, Li Q, Niu L, Xu L, Guo Y, Wang L and Guo C. Suppression of G6PD induces the expression and bisecting GlcNAc-branched N-glycosylation of E-cadherin to block epithelial-mesenchymal transition and lymphatic metastasis. Br J Cancer 2020; 123: 1315-1325.

[19] Wang Y, Li Q, Xu L, Chen J, Pu Y, Wang L, Sun H, Guo Y and Guo C. Cancer stemness of CD10-positive cells regulated by hedgehog pathway promotes the resistance to cisplatin in oral squamous cell carcinoma. Oral Dis 2020; [Epub ahead of print].

[20] Wang X, Feng J, Xue Y, Guan Z, Zhang D, Liu Z, Gong Z, Wang Q, Huang J, Tang C, Zou T and Yin P. Structural basis of N(6)-adenosine methylation by the METTL3-METTL14 complex. Nature 2016; 534: 575-578.

[21] Śledź P and Jinek M. Structural insights into the molecular mechanism of the m(6)A writer complex. Elife 2016; 5: e18434.

[22] Huang J, Dong X, Gong Z, Qin LY, Yang S, Zhu YL, Wang X, Zhang D, Zou T, Yin P and Tang C. Solution structure of the RNA recognition domain of METTL3-METTL14 N(6)-methyladenosine methyltransferase. Protein Cell 2019; 10: 272-284.

[23] Liu J, Yue Y, Han D, Wang X, Fu Y, Zhang L, Jia G, Yu M, Lu Z, Deng X, Dai Q, Chen W and He C. A METTL3-METTL14 complex mediates mammalian nuclear RNA N6-adenosine methylation. Nat Chem Biol 2014; 10: 93-95.

[24] Sato H, Nomura S, Maebara K, Sato K, Tamba M and Bannai S. Transcriptional control of cystine/glutamate transporter gene by amino acid deprivation. Biochem Biophys Res Commun 2004; 325: 109-116.

[25] Sasaki H, Sato H, Kuriyama-Matsumura K, Sato K, Maebara K, Wang H, Tamba M, Itoh K, Yamamoto M and Bannai S. Electrophile response element-mediated induction of the cystine/glutamate exchange transporter gene expression. J Biol Chem 2002; 277: 44765-44771.

[26] Jiang L, Kon N, Li T, Wang SJ, Su T, Hibshoosh H, Baer R and Gu W. Ferroptosis as a p53-mediated activity during tumour suppression. Nature 2015; 520: 57-62.

[27] Wang Y, Yang L, Zhang X, Cui W, Liu Y, Sun QR, He Q, Zhao S, Zhang GA, Wang Y and Chen S. Epigenetic regulation of ferroptosis by H2B monoubiquitination and p53. EMBO Rep 2019; 20: e47563.

[28] Martin L and Gardner LB. Stress-induced inhibition of nonsense-mediated RNA decay regulates intracellular cystine transport and intracellular glutathione through regulation of the cystine/glutamate exchanger SLC7A11. Oncogene 2015; 34: 4211-4218.

[29] Drayton RM, Dudziec E, Peter S, Bertz S, Hartmann A, Bryant HE and Catto JW. Reduced

expression of miRNA-27a modulates cisplatin resistance in bladder cancer by targeting the cystine/glutamate exchanger SLC7A11. Clin Cancer Res 2014; 20: 1990-2000.

[30] Huang H, Weng H, Sun W, Qin X, Shi H, Wu H, Zhao BS, Mesquita A, Liu C, Yuan CL, Hu YC, Hüttelmaier S, Skibbe JR, Su R, Deng X, Dong L, Sun M, Li C, Nachtergaele S, Wang Y, Hu C, Ferchen K, Greis KD, Jiang X, Wei M, Qu L, Guan JL, He C, Yang J and Chen J. Recognition of RNA N(6)-methyladenosine by IGF2BP proteins enhances mRNA stability and translation. Nat Cell Biol 2018; 20: 285-295.

[31] Zhang P, Wang W, Wei Z, Xu LI, Yang X and Du Y. xCT expression modulates cisplatin resistance in Tca8113 tongue carcinoma cells. Oncol Lett 2016; 12: 307-314.

[32] Lee JR, Roh JL, Lee SM, Park Y, Cho KJ, Choi SH, Nam SY and Kim SY. Overexpression of cysteine-glutamate transporter and CD44 for prediction of recurrence and survival in patients with oral cavity squamous cell carcinoma. Head Neck 2018; 40: 2340-2346.

[33] Yu D, Liu Y, Zhou Y, Ruiz-Rodado V, Larion M, Xu G and Yang C. Triptolide suppresses IDH1-mutated malignancy via Nrf2-driven glutathione metabolism. Proc Natl Acad Sci U S A 2020; 117: 9964-9972.

[34] Koppula P, Zhuang L and Gan B. Cystine transporter SLC7A11/xCT in cancer: ferroptosis, nutrient dependency, and cancer therapy. Protein Cell 2020; [Epub ahead of print].

The mechanism of METTL3-IGF2BP2-SLC7A11 axis in OSCC development

Table S1. The indicated sequences of siRNA and shRNA

Name	Sequence
siMETTL3#1	CAAGTATGTTCACTATGAA
siMETTL3#2	GACTGCTCTTTCCTTAATA
siIGF2BP1#1	GGCTCAGTATGGTACAGTA
siIGF2BP1#2	TGAAGATCCTGGCCCATAA
siIGF2BP2#1	CATGCCGCATGATTCTTGA
siIGF2BP2#2	GAACGAACTGCAGAACTTA
siIGF2BP3#1	GCTGAGAAGTCGATTACTA
siIGF2BP3#2	TAAGGAAGCTCAAGATATA
shMETTL3	5'-GATCCGGAGGAGTGCATGAAAGCCAGTGATTT
	CAAGAGAATCACTGGCTTTCATGCACTCCTCCTTTTTTG-3'

Table S2. The information of primary antibodies

Antibody name	Brand	Catalog number
GAPDH	Abclonal	A19056
METTL3	Abcam	ab195352
IGF2BP2	Abcam	ab128175
IGF2BP3	Abcam	ab177477
m^6A	Abcam	ab208577
SLC7A11	CST	12691S
pan-CK	Zhongshan Biosciences Inc.	ZM-0069

Table S3. The sequence of the primers used in qPCR

Primer name	Forward primer (5'→3')	Reverse primer (5'→3')
GAPDH	GACAGTCAGCCGCATCTTCT	GCGCCCAATACGACCAAATC
METTL3	CCAGCACAGCTTCAGCAGTTCC	GCGTGGAGATGGCAAGACAGATG
ADM2	CTGAGCCCCATCTGAAGCC	CAGCACTGCGTGTAGACCAG
ALDH1L2	TCTCCACTGGCCGGGTTTAT	CTTGCCCTTGACCCTCCATT
ASNS	TGAAGCATCGAGAGGGAACC	GACCGCGAAAATGTCCACAG
LAT2	ACAGAGCTTTACGGGGTCC	TGGGGTCTATGTAGGCTTCCT
PSAT1	TGGAGCCCCAAAATAGAAGCA	TCCCACAGACCTATGCCCTT
SLC7A11	TGGGACAAGAAACCCAGGTG	TCCCTATTTTGTGTCTCCCCTTG
IGF2BP1	GGCCATCGAGAATTGTTGCAG	CCAGGGATCAGGTGAGACTG
IGF2BP2	GGAACAAGTCAACACAGACACA	AACTGATGCCCGCTTAGCTT
IGF2BP3	ACTGCACGGGAAACCCATAG	ACTATCCAGCACCTCCCACT
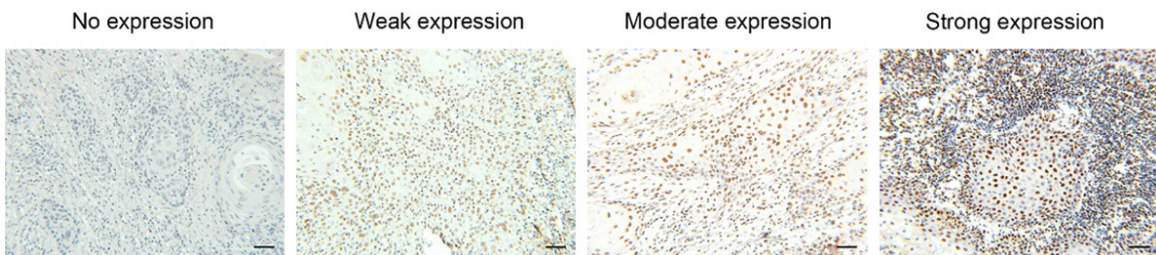
Figure S1. The expression pattern of METTL3 in OSCC samples (100×, scale bar: 100 μm).